

Static SU(3) potentials for sources in various representations

Sedigheh Deldar

Washington University, St. Louis, MO, 63130

(June 29, 2021)

The potentials and string tensions between static sources in a variety of representations (fundamental, 8, 6, 15-antisymmetric, 10, 27 and 15-symmetric) have been computed by measuring Wilson loops in pure gauge $SU(3)$. The simulations have been done primarily on anisotropic lattices, using a tadpole improved action improved to $O(a_s^4)$. A range of lattice spacings (0.43 fm, 0.25 fm and 0.11 fm) and volumes ($8^3 \times 24$, $10^3 \times 24$, $16^3 \times 24$ and $18^3 \times 24$) has been used in an attempt to control discretization and finite volume effects. At intermediate distances, the results show approximate Casimir scaling. Finite lattice spacing effects dominate systematic error, and are particularly large for the representations with the largest string tensions.

I. INTRODUCTION

One of the main goals of a non-perturbative formulation of gauge theories is to understand the phenomenon of confinement. According to the theory of confinement, the potential energy of a pair of heavy static quarks should increase linearly as a string or tube of flux is formed between them. For confined representations, one expects to see a Coulombic plus a linear term for the potential, $V(R) \simeq -A/R + KR + C$, where K is the string tension and R is the quark separation. For screened representations, $V(R)$ should level off at very large R , but one still expects the confined form for intermediate R with approximate Casimir scaling¹ of the string tension. Color screening must occur for adjoint quarks at sufficiently large separation, but it is very difficult to observe in numerical simulations, at least for zero temperature. The string tensions in various representations are basic properties of the pure non-Abelian gauge theory. To be viable, any theory of confinement (monopole condensation, center vortices,...) should thus be expected to reproduce the string tension in all representations.

The formation of a flux tube and the linear confinement of static quarks in the fundamental representation has been well established by pure gauge lattice QCD. The confinement of static sources in higher representations of QCD is still a question. Some numerical calculations have been done for SU(2) [2] and SU(3) [3] at non-zero temperature. At zero temperature, there have been studies for 8 (adjoint) [4,5], and 6 and 8 [6]. Preliminary results of the string tensions of some higher representations at zero temperature appear in [7,8]. Independent of this work, G. Bali has recently reported some results of the static source potentials of some higher representations [9,10].

In this paper, I give results for the potentials and string tensions of static sources of fundamental and some higher representations (6, 8, 15_a , 10, 27, 15_s) in pure SU(3). Most of the simulations have been done on anisotropic lattices with a tadpole improved action [11]. The main focus of this paper is the study of potentials at intermediate distances. I show that the potential in each representation at intermediate distances has a linear behavior and that the string tension is representation dependent and roughly proportional to the quadratic Casimir number.

II. CALCULATIONS

The string tension may be found by measuring the Wilson loops and looking for the area law falloff for large T , $W(R, t) \simeq \exp^{-V(R)T}$ where $W(R, T)$ is the Wilson loop as a function of R , the spatial separation of the quarks, and the propagation time T , and $V(R)$ is the gauge field energy associated with the static quark-antiquark source. The interquark energy for large separation grows linearly and for small separation is expected to be Coulombic, from single gluon exchange.

Direct measurement of Wilson loops for higher representations by multiplying the large matrices is not feasible considering the computer memory and the running time. One may expand the trace of Wilson loops for higher representations in terms of Wilson loops, U , in the fundamental representation. The higher representation states are

¹Here, the Casimir scaling means that the string tension for each representation is to be roughly proportional to the eigenvalue of the quadratic Casimir operator in that representation. The Casimir scaling regime is expected to exist for intermediate distances, perhaps extending from the onset of confinement to the onset of screening [1].

defined by the tensor product method. Let W be the higher representation counterpart to fundamental U for 6, 8, 10, 15-symmetric, 15-antisymmetric, or 27, then:

$$6 : tr(W) = 1/2 [(trU)^2 + trU^2], \quad (2.1)$$

$$8 : tr(W) = trU^*trU - 1, \quad (2.2)$$

$$10 : tr(W) = 1/6 [(trU)^3 + 2(trU^3) + 3trUtrU^2], \quad (2.3)$$

$$15s : tr(W) = 1/24 [(trU)^4 + 6(trU)^2trU^2 + 8trU(trU^3) + 3(trU^2)^2 + 6trU^4], \quad (2.4)$$

$$15a : tr(W) = 1/2trU^* [(trU)^2 + trU^2] - trU, \quad (2.5)$$

$$27 : tr(W) = 1/4[trU^2 + (trU)^2] [(tr(U^*))^2 + (trU^*)^2] - trUtrU^*, \quad (2.6)$$

where \star indicates complex conjugate.

III. SIMULATIONS

Two different improved actions are used for the lattice simulations, one for isotropic and the other one for anisotropic lattices. Using improved actions enables one to use coarser lattices and thereby to save computer time.

Calculating the static quark potential by measuring Wilson loops requires measurements at large enough T . Using a coarse isotropic lattice with fewer temporal sites than a usual fine lattice makes it difficult to measure quantities like the static quark potential. Anisotropic lattices, with a temporal lattice spacing smaller than the spatial one, make possible more measurements in the time direction. Since the signal to noise ratio of the correlation functions calculated in Monte Carlo simulations decays exponentially in time, having time slices closer together enables one to obtain more accurate results. The cost of simulations would still be less than the cost for fine lattices because of the coarseness of the spatial lattice spacings.

A. Isotropic lattice

The one-loop, tadpole-improved QCD gauge action of Ref. [12] is used for lattice simulations:

$$S[U] = \beta_{pl} \sum_{pl} \frac{1}{3} ReTr(1 - U_{pl}) + \beta_{rt} \sum_{rt} \frac{1}{3} ReTr(1 - U_{rt}) + \beta_{pg} \sum_{pg} \frac{1}{3} ReTr(1 - U_{pg}). \quad (3.1)$$

U_{pl} is the usual 1×1 plaquette operator, U_{rt} is the 1×2 rectangle operator, and U_{pg} is the six-link parallelogram operator (path $\mu, \nu, \rho, -\mu, -\nu, -\rho$ where μ, ν, ρ are all different directions). For this action the plaquette coupling is taken as an input and the other two couplings are computed using one-loop perturbation theory [13]:

$$\beta_{rt} = -\frac{\beta_{pl}}{20u_0^2} (1 + 0.4805\alpha_s), \quad (3.2)$$

$$\beta_{pg} = -\frac{\beta_{pl}}{u_0^2} 0.03325\alpha_s. \quad (3.3)$$

The mean link u_0 and the QCD coupling constant α_s are as follows:

$$u_0 = \left(\frac{1}{3} ReTr \langle U_{Pl} \rangle \right)^{\frac{1}{4}}, \quad (3.4)$$

$$\alpha_s = \frac{\frac{1}{3} \text{ReTr}(1 - \langle U_{pl} \rangle)}{3.06839}. \quad (3.5)$$

The discretization error is of order $O(\alpha_s^2 a^2, a^4)$.

Using this action, the fundamental representation static quark potentials for the following on- and off-axis points are found on a 8^4 lattice at $\beta_{pl} = 6.8$:

$$\vec{R} = (1, 0, 0), (2, 0, 0), (3, 0, 0), (4, 0, 0)$$

$$\vec{R} = (1, 1, 0), 2(1, 1, 0), (2, 1, 0), (1, 1, 1), (2, 1, 1), (2, 2, 1).$$

Summation over some possible paths from $(0,0,0)$ to the final destination points is done. This is a crude smearing. The averages are projected back to $SU(3)$.

B. Anisotropic lattice

The tadpole-improved tree level action of Ref. [11] is used for anisotropic lattices. The action has the form:

$$S = \beta \left\{ \frac{5}{3} \frac{\Omega_{sp}}{\xi u_s^4} + \frac{4}{3} \frac{\xi \Omega_{tp}}{u_s^2 u_t^2} - \frac{1}{12} \frac{\Omega_{sr}}{\xi u_s^6} - \frac{1}{12} \frac{\xi \Omega_{str}}{u_s^4 u_t^2} \right\}, \quad (3.6)$$

where $\beta = 6/g^2$, g is the QCD coupling, and ξ is the aspect ratio ($\xi = a_s/a_t$ at tree level in perturbation theory). Ω_{sp} and Ω_{tp} include the sum over spatial and temporal plaquettes; Ω_{sr} and Ω_{str} include the sum over 2×1 spatial rectangular and short temporal rectangular (one temporal and two spatial links), respectively. For $a_t \ll a_s$ the discretization error of this action is $O(a_s^4, a_t^2, a_t a_s^2)$. The coefficients are determined at tadpole-improved tree level [14]. The spatial mean link, u_s , is given by:

$$\left\langle \frac{1}{3} \text{ReTr} P_{ss'} \right\rangle^{\frac{1}{4}}, \quad (3.7)$$

where $P_{ss'}$ denotes the spatial plaquette. In general the temporal link u_t can be determined from:

$$u_t = \frac{\sqrt{\frac{1}{3} \langle \text{ReTr} P_{st} \rangle}}{u_s}, \quad (3.8)$$

where P_{st} is the spatial-temporal plaquette. When $a_t \ll a_s$, u_t , the temporal mean link can be fixed to $u_t = 1$, since its value in perturbation theory differs by unity by $O(\frac{a_t^2}{a_s^2})$.

Measurements are done on four lattices $10^3 \times 24$, $8^3 \times 24$, $18^3 \times 24$, and $16^3 \times 24$ at β equal to 1.7, 2.4, 2.4 and 3.1 with aspect ratios of 5, 3, 3, and 1.5, respectively. The temporal lattice spacings are kept approximately the same. For the last lattice, $16^3 \times 24$ at $\beta = 3.1$, the aspect ratio is 1.5, which means the spatial lattice spacing is only 1.5 times bigger than the temporal lattice spacing. Therefore u_t is calculated directly from Eq. (3.8).

u_s and u_t are spatial and temporal renormalization factors introduced by mean field theory (“tadpole improvement”). Mean field theory allows one to sum the effects of the largest higher order contributions and thereby significantly improve the reliability of perturbation theory.

At finite coupling, the anisotropy $\frac{a_s}{a_t}$ is renormalized away from its input value ξ . Measurements of this renormalization can be made by using the static quark potential extracted from correlations along the different spatial and temporal axes of the lattice [11]. The renormalization can be as large as 30% without doing mean-link improvement. With mean-link improvement, the difference is found to be typically a few percent. In this work, I ignore the small radiative corrections to the aspect ratio $\xi = \frac{a_s}{a_t}$. This includes additional small lattice spacing errors which however vanish as $a_s \rightarrow 0$.

C. Smearing

Smearing on spatial links is performed to minimize the excited state contaminations in the correlation functions. In other words, by smearing one can produce an interpolating field which has greater overlap with the ground state

and smaller overlap with excited states. In the smearing procedure each link is replaced by itself plus a sum of its four neighboring spatial staples times a smearing factor λ [15] (APE smearing):

$$U_j(x) = P_{su(3)}\{U_j(x) + \lambda \sum_{\pm k \neq j} U_k(x)U_j(x + \hat{k})U_k^\dagger(x + \hat{j})\}. \quad (3.9)$$

λ is the smearing factor and P indicates the projection back to $SU(3)$. Projection back to $SU(3)$ after smearing or after averaging over different paths in Wilson loops is necessary, in order to use Eqs. (2.1) to (2.6), in which the U 's must be $SU(3)$ matrices. For the same reason thermal averaging is not possible, since again it would take links out of $SU(3)$. (Thermal averaging, which is normally useful to increase statistics, is the replacement of a time-like link by its average with fixed neighbors.) The smearing factor, λ , is kept the same for all lattice distances but the smearing levels (number of smearings) are chosen separately for each distance from some low statistics runs. With trial and error, one can optimize the smearing factor and smearing level. Here ‘‘optimize’’ means to find a good plateau with good statistics at the smallest possible value of T . In general for a given lattice, the smearing level and the smearing factor are smaller for smaller R . For large distance potentials, the configuration of glue appears to spread out more, and more smearing is needed. As a general rule, the finer the lattice spacing, the larger the smearing level needed, so that the smearing extends out to a comparable physical distance.

Projection back to $SU(3)$ is done by maximizing $tr(UV^\dagger)$, where U is the normalized smeared link (in $SU(3)$) and V is the unnormalized smeared link. V does not belong to $SU(3)$ since it is obtained by summing the $SU(3)$ links (Eq. 3.9). $U = \frac{V}{\det(V)}$ minimizes $tr(UV^\dagger)$ in $SU(2)$, because the sum of $SU(2)$ matrices is proportional to an $SU(2)$ matrix. To do this in $SU(3)$, one loops over several embeddings of the $SU(2)$ subgroups in the $SU(3)$ matrix; U converges iteratively to the right answer.

D. Fitting codes for analyzing the Wilson loops

To take the auto-correlation length into account, the Wilson loops are grouped into blocks. The appropriate block size is determined by j_0 , demanding that the plaquette auto-correlation function fall near zero after j_0 measurements. The error is stable under blocking with size $j > j_0$. Using this method, the appropriate block size has been chosen for each lattice simulation.

Two fitting codes are used for computing the potentials and the string tensions. The first code fits the Wilson loops of each fixed R to the exponential form:

$$W \simeq \exp^{-V(R)T}$$

and finds the static quark potential $V(R)$ at each lattice distance R . Fig. 1 shows a typical plot, obtained by the first fit, of the potential between two static sources in representation 8 (adjoint) for the lattice distance $\vec{R} = (2, 2, 2)$. The measurements in this figure have been obtained on an $8^3 \times 24$ lattice. The fit range, which is chosen individually for each R , shows the plateau region. The errors of the fitting parameters are found by the jackknife method. Q , the confidence level for each fit, is calculated by measuring the covariance matrix evaluated by jackknife.

The potentials obtained by the first fit are then used to fit the potential to the form:

$$V(R) \simeq -A/R + KR + C. \quad (3.10)$$

The results of the first fits are computed for all jackknife subensembles, and therefore the jackknife errors of the second fit parameters can be computed. The string tension, Coulombic coefficient, and the constant in lattice units are the result of the second fit.

To have a better estimate of the covariance matrix, one can try to eliminate its unreliable eigenvalues and eigenvectors [16]. Suppose we have N independent blocks of Wilson loops for a fixed R . The average of Wilson loops at time T_i is called \bar{w}_i :

$$\bar{w}_i = \frac{1}{N} \sum_k w_{ik}, \quad (3.11)$$

where w_{ik} is the result for the k th block. Then the covariance matrix is defined as:

$$C_{ij} = \frac{1}{N-1} \left(\frac{1}{N} \sum_{k=1}^N (w_{ik} - \bar{w}_i)(w_{jk} - \bar{w}_j) \right). \quad (3.12)$$

It is then convenient to define the correlation matrix:

$$P_{ij} = \frac{C_{ij}}{\sqrt{C_{ii}C_{jj}}}. \quad (3.13)$$

The diagonal elements of P are equal to 1 and all the others are less than 1. Call the eigenvalues of the correlation matrix ρ_a . Then $\sum_a \rho_a = n$ for the $n \times n$ correlation matrix. The average eigenvalue is thus 1. The small eigenvalues $\rho_a \ll 1$ (or even $\rho_a < 1$) are often poorly determined with a finite data set. These may give a false estimation of the covariance matrix. One can make a new correlation matrix out of only those eigenvectors whose eigenvalues are greater than some cutoff:

$$P' = B + D, \quad (3.14)$$

where

$$B = \sum'_a \rho_a |\psi_a\rangle\langle\psi_a|, \quad (3.15)$$

and

$$D_{ij} = \delta_{ij}(1 - B_{ii}). \quad (3.16)$$

The prime on the sum in Eq. (3.15) indicates that the sum is over a subset of the eigenvectors: those whose eigenvalues are greater than the cutoff. Now $(C'_{ij})^{-1}$, which is the inverse of the modified covariance matrix, is given by:

$$(C'_{ij})^{-1} = \frac{(P'_{ij})^{-1}}{\sqrt{C_{ii}C_{jj}}}, \quad (3.17)$$

and

$$C'_{ij} = P'_{ij} \sqrt{C_{ii}C_{jj}}. \quad (3.18)$$

If the cutoff is taken greater than the maximum eigenvalue, then C' would be a diagonal matrix, with the diagonal elements equal to the standard errors, and the fit would be an uncorrelated fit. This method thus interpolates between correlated and uncorrelated fits. In general, I keep the complete covariance matrix in computing Q . However, in some cases the small eigenvalues of the covariance matrix are poorly determined (due to limited statistics), and I am forced to drop these eigenvalues and the corresponding eigenvectors.

E. Setting the scale

I use the hadronic scale r_0 , determined from the force between static quarks at intermediate distance [17], to set the lattice scale. r_0 is defined by:

$$\left[r^2 \frac{dV(\vec{r})}{dr} \right]_{r=r_0} = 1.65, \quad (3.19)$$

where $V(\vec{r})$ is the static quark potential in the fundamental representation. The definition of Eq. (3.19) gives $r_0 \simeq 0.5$ fm in a phenomenological potential model. In this work I use $r_0^{-1} = 410 \pm 20$ MeV determined by Morningstar [11]. This value is an average of r_0 from various quenched lattice simulations in which the quantities such as the mass of the ρ or the $1P$ - $1S$ splitting in heavy quarkonia are used to set the lattice spacing. To fix a_s , the spatial lattice space, I thus use (see Eqs. (3.10) and (3.19)):

$$\frac{r_0}{a_s} = \sqrt{\frac{1.65 - A}{K a_s^2}}. \quad (3.20)$$

For the anisotropic action I measure $K a_s a_t$ from the fits. To compute $K a_s^2$, I have to know the aspect ratio $\xi = \frac{a_s}{a_t}$. I use the input value of ξ , since the difference between the input value and what one computes from the lattice

simulation vanishes in the continuum limit and is expected to be small at these lattice spacings [11]. The scaling of the fundamental string tension is good evidence that this expectation is correct.

Using the scaled potentials and lattice distances in terms of the hadronic scale r_0 , it is possible to show the results of different lattice simulations in one plot. For example see Fig. 2, where $r_0[V(r) - V(2r_0)]$ for the fundamental representation is plotted versus $\frac{r}{r_0}$. All other physical quantities can be computed in terms of the scale r_0 and can then be expressed in relevant physical units using the value of r_0 from other lattice simulations. The scaled potentials for the higher representations can be plotted by using the lattice spacing in terms of the hadronic scale of the fundamental representation (see Fig. 2 for representation 8).

F. Computers and simulation codes

In the first stage of this work, I have used code I have written in the computer language C for simulations on isotropic lattices. Later, to decrease the running time of the codes, I have used the MILC Collaboration software as a platform [18]. The results obtained by my previous codes on the isotropic lattices are in agreement with the results of the MILC platform codes.

The simulations have been done on a Dec Alpha and on Origin 2000's supercomputers (single node jobs).

IV. RESULTS AND DISCUSSION

A. Isotropic Lattice

Using the improved action, Eq. (3.1), the static quark potentials for the fundamental representation have been found on an 8^4 lattice at plaquette coupling constant, β_{pl} , equal to 6.8. Other input parameters such as the rectangle and parallelogram coupling constants, have been computed from Eqs. (3.2) to (3.5) ($\beta_{rt} = -0.562$, $\beta_{pg} = -0.0844$).

Fig. 3 represents the result of fitting the potentials to the form of Eq. (3.10). The violation of rotational invariance indicated by the deviation of the off-axis potentials from the fit is about 3 – 8%, while with the same lattice spacing, this deviation is as much as 35% with Wilson action. This deviation is due to finite lattice spacing errors. The dimensionless string tension given by this fit is equal to 0.784(6). By comparing this value with the phenomenological value of the string tension $(420\text{MeV})^2$, I find a lattice spacing of approximately 0.42 fm.

B. Anisotropic Lattice

The simulations are performed for three coupling constants based on the approximate desired spatial lattice spacing ratios 4:2:1. The aspect ratios have been chosen such that the temporal spacings are approximately the same in all lattices. Two lattice sizes for $\beta = 2.4$, one for $\beta = 1.7$ and one for $\beta = 3.1$ are studied. The renormalization factors for spatial and temporal links, u_s and u_t , have been computed for each β . Table I shows the input parameters used in the simulations. The number of configurations represents the number of measured Wilson loops for each R and T . The last column of Table I shows the number of blocks for each calculation.

For all lattices except the $8^3 \times 24$ lattice, only on-axis potentials have been measured. On $8^3 \times 24$, the potentials have been calculated for the following distances:

$$\vec{R} = (1, 0, 0), (2, 0, 0), (3, 0, 0), (4, 0, 0)$$

$$\vec{R} = (1, 1, 0), 2(1, 1, 0), (2, 1, 0), (1, 1, 1), 2(1, 1, 1), (2, 1, 1), (2, 2, 1).$$

In each lattice updating, three over-relaxation steps and one Metropolis step are performed. Each Metropolis step includes 15 hits on $SU(2)$ subgroups. Lattice measurements are done every three updates for $\beta = 1.7$ and $\beta = 2.4$, and every four updates for $\beta = 3.1$.

The potential at distance R is determined from the asymptotic behavior of Wilson loops, $W(R, T)$:

$$V(R) \simeq \lim_{T \rightarrow +\infty} \ln\left(\frac{W(R, T)}{W(R, T+1)}\right)$$

Wilson loops have been fitted to the exponential form of the above equation, and $V(R)$ times the temporal lattice spacing has been found.

To extract the potential from the Wilson loops, one has to measure the Wilson loops for large values of R and T . To minimize the excited state contribution and to find the static potential, one has to measure the Wilson loops for large T 's. With the current statistics of this work (Table I), it is possible to go to large enough T values to measure the Wilson loops in lower representations and for small and even intermediate R in higher representations. For large R values — especially for higher representations — the Wilson loops get too small for large T , and the error due to statistical fluctuations makes the measurements meaningless. Because of the lack of data for large values of T , I have therefore had to calculate the potentials using small T 's. However, I have been able to estimate the systematic error by changing the fit range or by comparing with V of smaller R 's. In most cases, it is still possible to get a good confidence level, Q , after changing the fit range by one or two units in T_{\min} . The comparison of the results for different values of T_{\min} gives an estimate of the systematic error from excited states. However, for large values of R , the T_{\min} 's are usually very small. In these cases the systematic error due to moving the plateau is taken from V at smaller R . I take the error on the potential as the sum in quadrature of statistical and systematic errors. The systematic error is due to change of the fit range.

The potentials obtained by fitting the Wilson loops to an exponential form are then used to fit $V(R)$ versus R . A Gaussian distribution of the systematic error due to the change of the fit range of the fits V versus T is added to the potentials. Then the modified data sets (potentials) from the first fits are fitted to a Coulombic plus a linear term of Eq. (3.10). As a result of this correlated fit, the coefficient of the Coulombic term, A , the string tension times the square of spatial lattice spacing, $K a_s^2$, and the constant term are found. The string tension in terms of the hadronic scale r_0 is measured as well. Fig. 4 shows $a_t V$ versus R (in units of a_s) for fundamental, 6, 8, 15-antisymmetric, 10, 27 and 15-symmetric dimensional representations for $8^3 \times 24$ lattice at $\beta = 2.4$. Only on-axis points are used in the fits. Off-axis potentials deviate from the fit about 2%-8%; these are evidence for rotational non-invariance — a systematic error due to finite a_s . Fig. 5 shows the plot of $a_t V$ of various representations versus lattice distance R for $\beta = 2.4$ ($18^3 \times 24$ lattice). The confidence levels of the fits are indicated by Q 's. The error bars on the points are the sum in quadrature of statistical and systematic errors due to change of the fit range in T . The slopes of the potentials are qualitatively in agreement with Casimir scaling. The fundamental-representation results from the fits of V versus R for different lattices are shown in Table II. In this Table the spatial lattice spacing a_s in terms of r_0 is given for different lattices. The temporal lattice spacing, a_t , can be found by aspect ratio, $\xi = a_s/a_t$.

Figs. 2 and 6 show the static quark potential of some representations in terms of the hadronic scale for $\beta = 1.7$, $\beta = 2.4$ and $\beta = 3.1$. The dimensionless string tension, $K r_0^2$, for each β and the best estimate for each representation are presented. A shows the dimensionless Coulombic coefficient. The best estimate for the string tension of each representation is obtained by the weighted average of the four lattice measurements. The errors in the string tensions are the statistical error (from the weighted average) and the systematic error of discretization (determined by the standard deviation of the results over the 3 couplings), and the error on r_0 , respectively. Table III gives $K r_0^2$ for different β 's and the best estimate of the dimensionless string tension. In Table IV the ratio of the string tension of each representation to the fundamental one is given. There is a rough agreement between these ratios and the Casimir number ratios of higher representations to the fundamental one as predicted [19]. The fundamental representation string tension, 0.222(1)(8)(21) GeV, is in reasonable agreement with the phenomenological value of 0.18(2) GeV. (Note that the value used here for r_0 , $r_0^{-1} = 410 \pm 20$ MeV, is determined without reference to the string tension [11].) Based on the best estimate of the string tension given by Table IV, $K_s/K_f = 1.97(1)(12)$. This ratio is in agreement with 2.2(4) reported by Campbell *et al.* [4].

The Coulombic coefficients (A), the best estimate of the A 's found by weighted average, and the ratios of the average A of each representation to the the fundamental one are given in Table V. Comparing the ratios with Casimir ratios, one can see some qualitative agreement, although there are some large disagreements for a few of the representations. The value of the Coulombic coefficient, A , is quite sensitive to the lower bound of the fit range. That is why it shows some differences among different lattices. The weighted average of the fundamental Coulombic coefficient, A , from Table II is equal to .329(4)(49). This is about 2σ off from $\frac{\pi}{12}$ of the standard infrared parametrization form of the static quark potential:

$$V(R) \simeq -\pi/12 + KR + C.$$

For the fundamental representation, good scaling behavior (results independent of lattice spacing) is observed. The scaling gets worse for higher representations, roughly in proportion to the string tension. It seems that the higher representations are more sensitive to the lattice spacing although it is difficult to make a definitive statement because the data get progressively worse as the dimension of the representation increases. With the current data, the string tensions of the higher representations at intermediate lattice spacing ($\beta = 2.4$) are actually closer to the result at the coarsest lattice spacing ($\beta = 1.7$) than they are to the result of the finest lattice spacing ($\beta = 3.1$). Scaling errors are the most important systematic error in this study.

Screening or a change of the slope should start to show up when the potential energy of the static quarks becomes equal to or larger than twice the glue-lump mass. As a result, a pair of gluons pops out of vacuum which interact with the static sources and cause screening or a changing of the potential slope, depending on the triality of the representation. The horizontal dotted line in Fig. 2 shows twice the glue-lump potential. The static potential energy of the two adjoint sources becomes equal to $2 \times M_{glueball}$ at about 1.2 fm [6]. This energy is enough to pop out two octets. In the current work, no change of the slope of the linear part of the potential for representations 6, 15-antisymmetric and 15-symmetric is observed yet (they can in principle be converted into the fundamental representation by dynamical gluons). No screening for representations 8, 10, 27 is seen either. (These representations have zero triality and can in principle be screened by dynamic gluons.) This is not surprising, given the well known fact that the Wilson loops do not couple well to screened states. Presumably one would need additional sources which couple better to separated screened states (see, e.g.,) [20] and [21]) to see the screening at reasonable values of R . Wilson loops couple primarily to string-like, confined states.

Using the hadronic scale r_0 given by $r_0^{-1} = 410 \pm 20$ MeV [11], one can calculate the lattice spacings in energy units. The spatial lattice spacings are then 0.43(1)(2) fm, 0.2482(6)(101) fm, 0.2509(5)(102) fm, and 0.1072(5)(44) fm for lattices $10^3 \times 24$, $8^3 \times 24$, $18^3 \times 24$, and $16^3 \times 24$ at β equal to 1.7, 2.4, 2.4, and 3.1, respectively. The first error of each lattice spacing is the error from this work and the second error is due to the hadronic scale uncertainty.

The finite volume effect is studied by measuring the Wilson loops on the two lattice sizes $8^3 \times 24$ and $18^3 \times 24$ for $\beta = 2.4$. The potentials are generally in agreement; in a very few cases a slight difference is observed (not more than 6%). The scaled string tensions, Kr_0^2 , of Table III are also in good agreement for the two lattices. A difference of at most 2σ is observed for some representations. This can be explained as a result of a different fit range for the smaller lattice. In other words, for the bigger lattice, $18^3 \times 24$, larger distances have a more significant role in determining the string tension. In contrast, for the smaller lattice, $8^3 \times 24$, the fits are based on only four points. Since the physical volume at $\beta = 1.7$ and $\beta = 3.1$ are comparable to or larger than that at $8^3 \times 24$, $\beta = 2.4$, I conclude that the lattice volumes are big enough and the finite volume errors are much smaller than the dominant systematic error, which is due to discretization. Figs. 4 and 5 show the potentials and the string tensions for various representations for the two lattice sizes.

Another source of the systematic error is due to the finite lattice spacing in the time direction. The action used for the anisotropic lattice (Eq. (3.6)) has $O(a_s^4, a_t^2, \alpha_s a_s^2)$ discretization errors and is intended for use with $a_t \ll a_s$. As I take a_s smaller in this work, I keep a_t fixed. At $\beta = 3.1$, the aspect ratio, $\xi = \frac{a_s}{a_t}$ is only 1.5, so the $O(a_t^2)$ errors may no longer be negligible compared to the $O(a_s^4)$ errors, although they are expected to be small on an absolute scale.

V. CONCLUSION

The string tensions in various representations are basic properties of the pure non-Abelian gauge theory and therefore should be predicted in any theory of confinement for any representation. In this work, the static potentials for the fundamental and some higher representations have been studied by numerical lattice calculations. The results provide a test of confinement models.

By lattice calculations, the fundamental static potentials and the string tension have been computed by measuring the Wilson loops on an 8^4 isotropic lattice at $\beta_{pl} = 6.8$. The one-loop, tadpole-improved QCD gauge action has been used. Both on- and off-axis potentials have been measured, and the effect of the coarse lattice has been discussed. It has been found that the violation of rotational invariance indicated by the deviation of the off-axis potentials from the fit is only about 3 – 8%. This makes the improved action a useful tool in lattice calculations.

The fundamental and higher representation potentials and the string tensions have been computed on four anisotropic lattices using a tadpole-improved tree level action. To extrapolate to the continuum and to study the volume effect, three lattice spacings with the approximate ratio of 1:2:4 on four lattice sizes have been studied. Lattice spacings range from 0.11 fm to 0.43 fm and the lattice sizes are $10^3 \times 24$, $8^3 \times 24$, $18^3 \times 24$, and $16^3 \times 24$ at β equal to 1.7, 2.4, 2.4, and 3.1, respectively. Using the hadronic scale r_0 , which is defined in terms of the potential between static quarks at an intermediate distance in the fundamental representation, the dimensionful string tensions have been calculated, and the scaling behavior has been studied. Good scaling behavior for the fundamental representation is observed. The scaling gets worse for higher representations, roughly in proportion to the string tension. At small and intermediate distances, rough agreement with Casimir scaling is observed.

VI. ACKNOWLEDGMENTS

I would like to thank Claude Bernard for his great support in this work. I wish to thank the MILC Collaboration and especially Robert Sugar and Steven Gottlieb for computing resources. Also I wish to thank J. Mandula, U. Heller and C. Morningstar for helpful discussions.

- [1] M. Faber, J. Greensite, S. Olejník, Phys. Rev. D57 (1998) 2603-2609.
- [2] C. Bernard, Phys. Lett. 108B (1982) 431; Nucl. Phys. B219 (1983) 341; J. Ambjørn, P. Olesen, C. Peterson, Nucl. Phys. B240 (1984) 189; C. Michael, Nucl. Phys. B259 (1985) 58; G. Poulis, H. Trotter, Phys. Lett. B400 (1997) 358.
- [3] S. Ohta, M. Fukugita, A. Ukawa, Phys. Lett. B173 (1986) 15; M.E. Faber, H. Markum, Nucl. Phys. B (Proc. Suppl.) 4 (1988) 204; M. Müller, W. Beirl, M. Faber, H. Markum, Nucl. Phys. B (Proc. Suppl.) 26 (1992) 423.
- [4] N.A. Campbell, I.H. Jorysz, C. Michael, Phys. Lett. 167B (1986) 91.
- [5] C. Michael, Nucl. Phys. B (Proc. Suppl.) 6 (1992) 417 .
- [6] C. Michael, hep-lat/9809211.
- [7] S. Deldar, Nucl. Phys. B (Proc. Suppl.) 73 (1999) 587.
- [8] S. Deldar, Nucl. Phys. B (Proc. Suppl.) 83-84 (2000) 440.
- [9] G.S. Bali, Nucl. Phys. B (Proc. Suppl.) 83-84 (2000) 422.
- [10] G.S. Bali, hep-ph/0001312.
- [11] C. Morningstar, Nucl. Phys. B (Proc. Suppl.) 53 (1997) 914.
- [12] M. Alford, W. Dimm, G.P. Lepage, G. Hockney, P.B. Mackenzie, Phys. Lett. B361 (1995) 87.
- [13] G.S. Bali, K. Schilling, Phys. Rev. D46 (1992)2636.
- [14] G.P. Lepage and P.B. Mackenzie, Phys. Rev. D48 (1993) 2250.
- [15] M. Albanese *et al.*, Phys. Lett. B192 (1987) 163.
- [16] C. Detar (private communication); H.H. Harmen, *Modern Factor Analysis*, 2nd ed. (Univ. of Chicago Press, Chicago 1967), Chap. 8.
- [17] R. Sommer, Nucl. Phys. B411 (1994) 839.
- [18] <http://physics.indiana.edu/~sg/milc.html>.
- [19] J. Ambjørn, P. Olesen, C. Peterson, Nucl. Phys. B240 (1984) 189.
- [20] P.W. Stephenson, Nucl. Phys. B550 (1999)427;
- [21] O. Philipsen, H. Wittig, Phys. Lett. B451 (1999) 146.

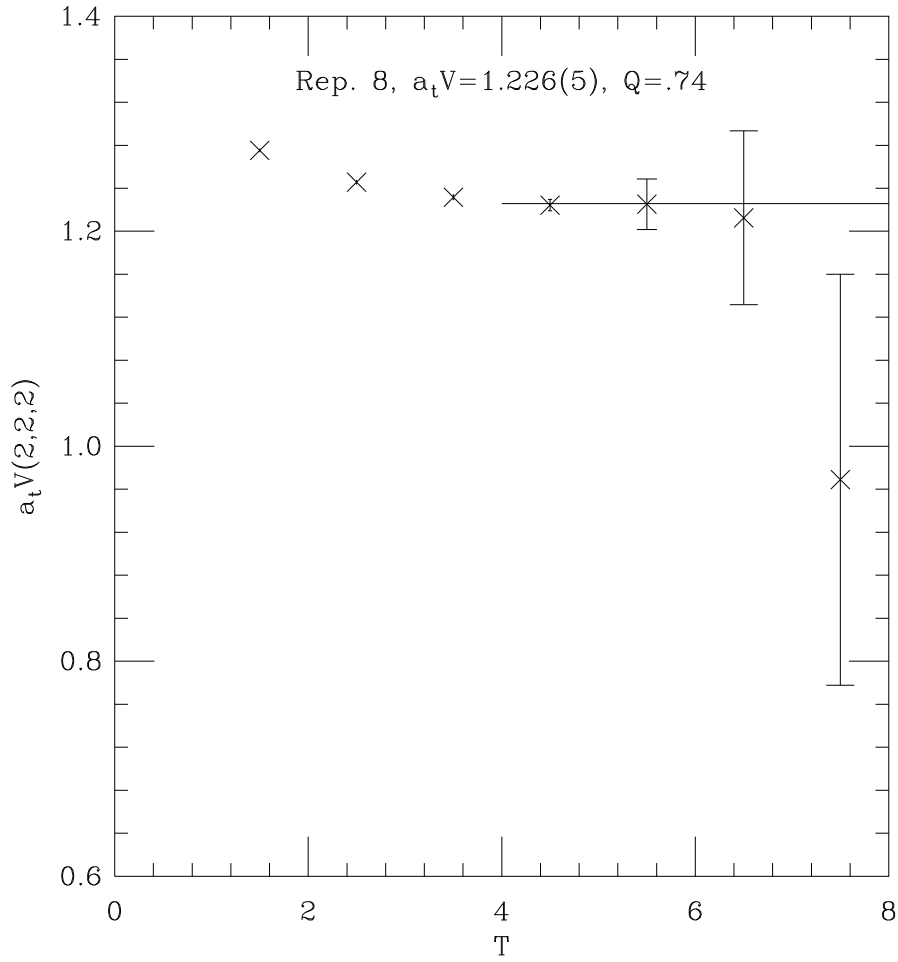


FIG. 1. $V(2, 2, 2)$ versus T for $8^3 \times 24$ lattice and $\beta = 2.4$. The fit range is shown by the solid line.

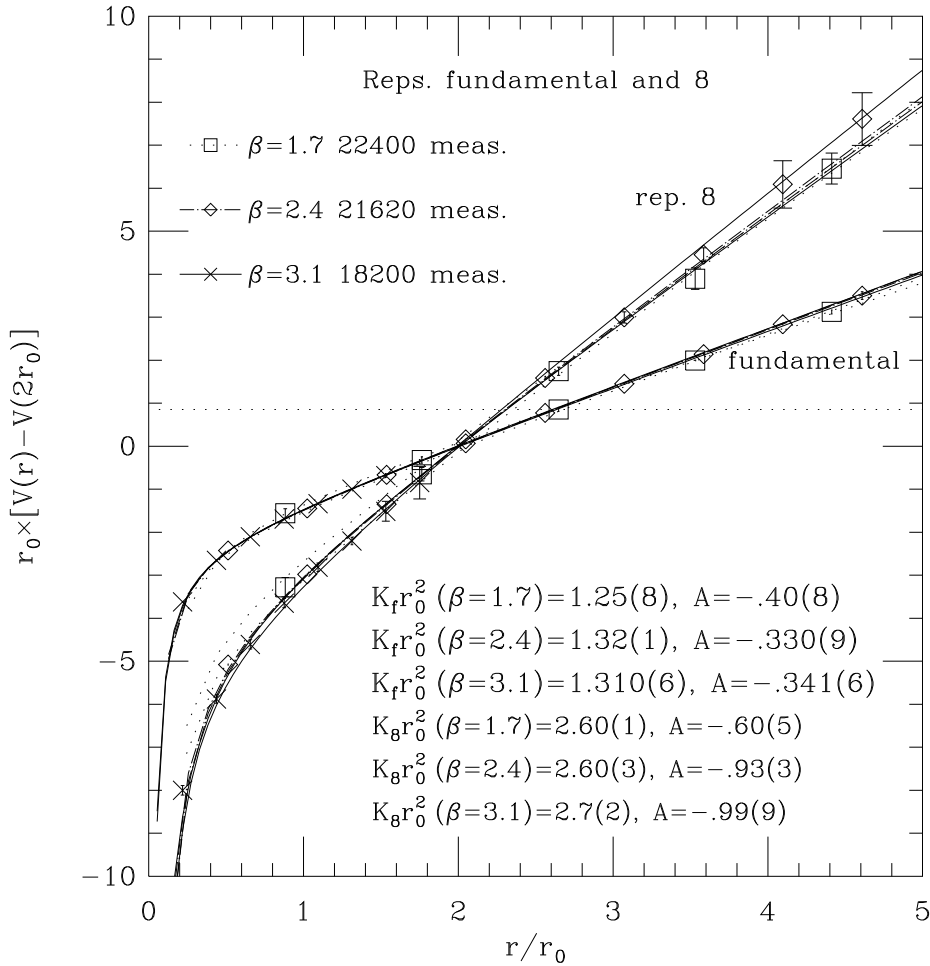


FIG. 2. The static quark potential $V(R)$ in terms of hadronic scale r_0 for representations fundamental and 8. The double line shows the central value of the fit \pm error. The horizontal dotted line shows the potential energy of glue-lumps. Good scaling behavior is observed. The weighted average string tensions for representations fundamental and 8 are $Kr_0^2=1.324(4)(51)$ and $Kr_0^2=2.602(9)(119)$, respectively.

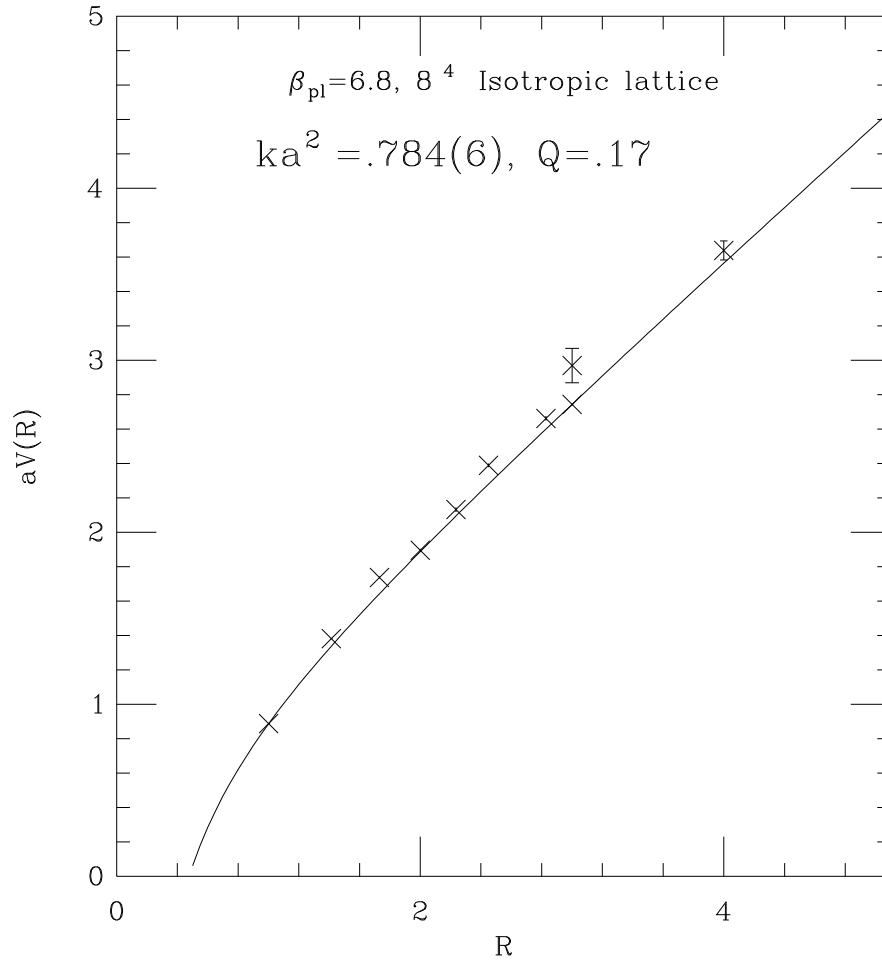


FIG. 3. Potential versus R for an 8^4 lattice at $\beta_{Pl} = 6.8$. Ka^2 shows the string tension times the square of the lattice spacing. A indicates the Coulombic coefficient. The off-axis points deviate from the fit by about 3 – 8%. Only on-axis points are used in the fit.

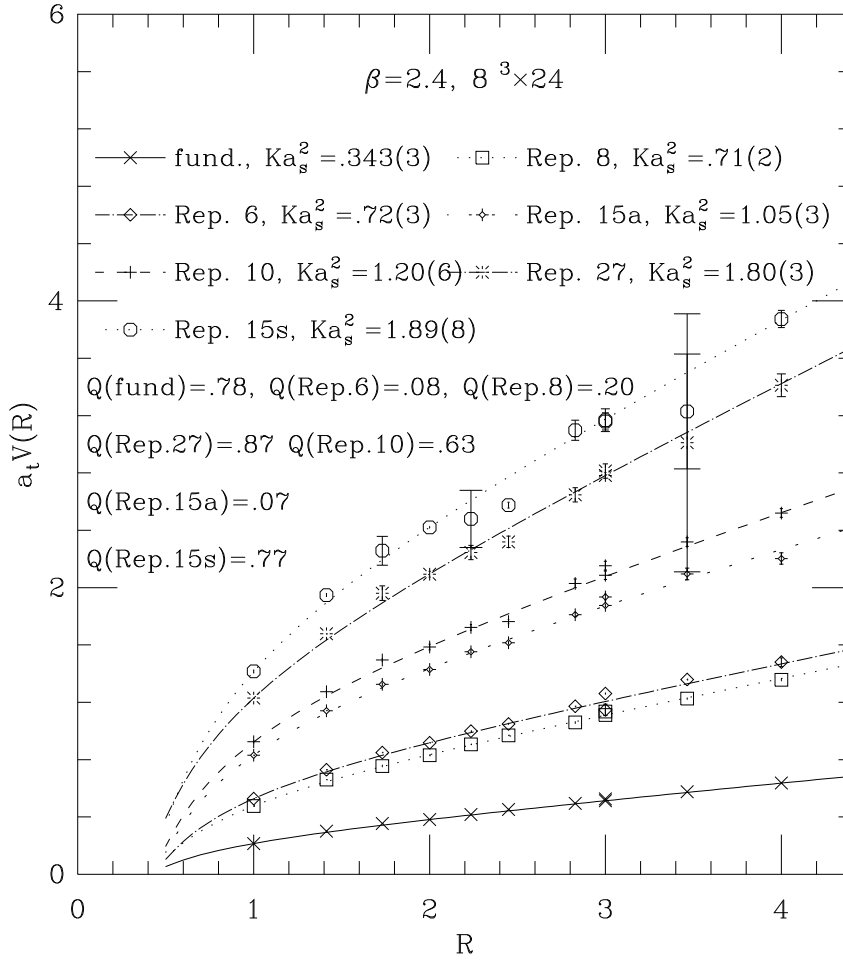


FIG. 4. A typical plot of $a_t V(R)$ versus R for various representations $8^3 \times 24$ lattice at $\beta = 2.4$. Ka_s^2 shows the string tension times the spatial lattice spacing square. The error bars on the points are the sum in quadrature of statistical and systematic errors. The systematic errors are due to a change of the fit range of V versus T .

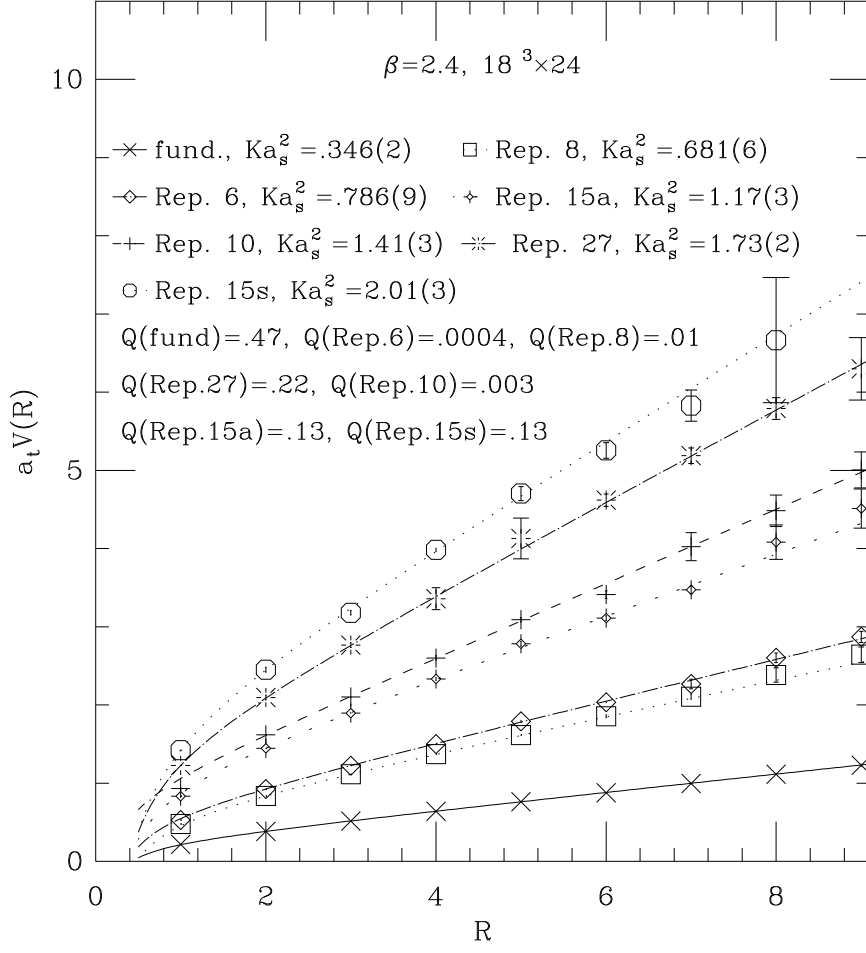


FIG. 5. Same as figure 4 but for the $18^3 \times 24$ lattice at $\beta = 2.4$.

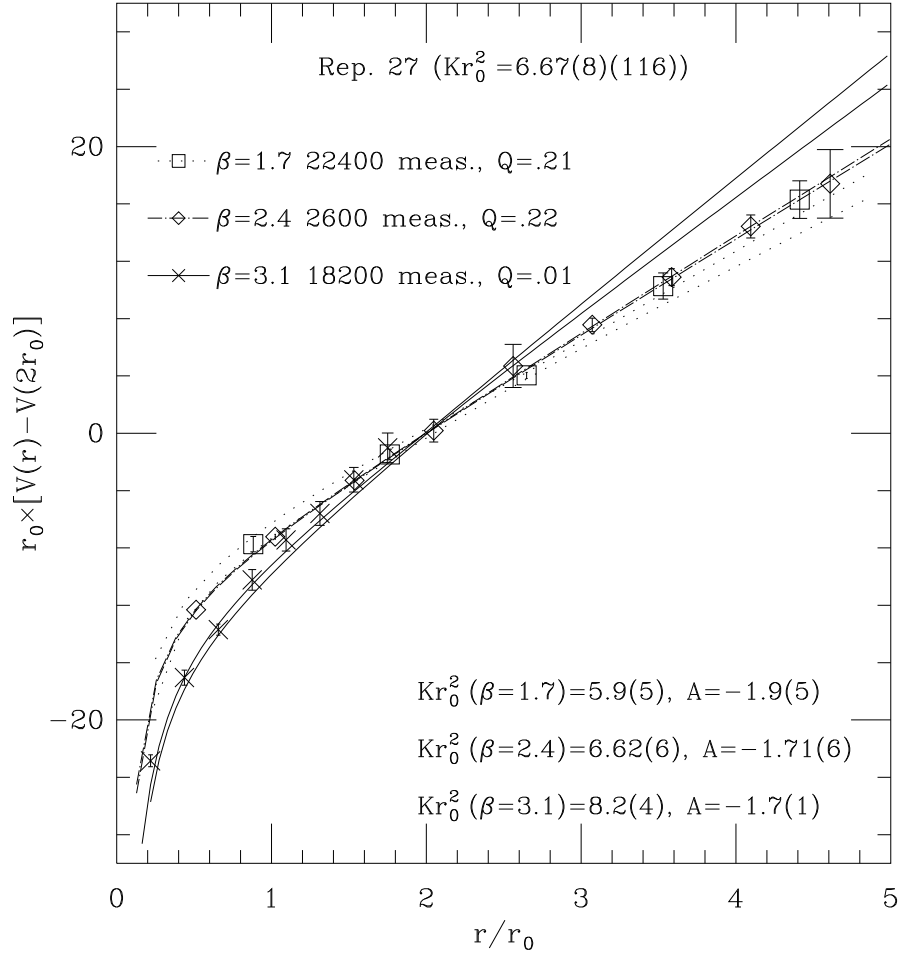


FIG. 6. Same as figure 2 but for representation 27. The final result is $Kr_0^2 = 6.67(8)(116)$.

TABLE I. Input parameters for lattice calculations. The renormalization factors for spatial and temporal links are given by u_s and u_t , respectively.

Lattice	β	u_s^4	u_t	# configs	# blocks
$10^3 \times 24$	1.7	.295	1.	22400	224
$8^3 \times 24$	2.4	.421	1.	7200 – 7900	50
$18^3 \times 24$	2.4	.421	1.	21620	188
$16^3 \times 24$	3.1	.575	.945	18200	182

TABLE II. Results of the fit of the fundamental potential to a Coulombic plus linear form. A shows the Coulombic coefficient and Cr_0 is the constant term times the hadronic scale r_0 . The fundamental string tension and the spatial lattice spacing in terms of r_0 are given as Kr_0^2 and r_0/a_s , respectively.

β	Lattice	ξ	r_0/a_s	A	Kr_0^2	Cr_0
1.7	$10^3 \times 24$	5.0	1.13(3)	-.40(8)	1.25(8)	.42(7)
2.4	$8^3 \times 24$	3.0	1.974(5)	-.315(6)	1.335(5)	1.22(2)
2.4	$18^3 \times 24$	3.0	1.953(4)	-.330(9)	1.32(1)	1.21(1)
3.1	$16^3 \times 24$	1.5	4.57(2)	-.341(6)	1.310(6)	3.07(3)

TABLE III. String tensions in terms of r_0 for different coupling constants, lattice sizes, and the best estimate.

Rep.	$Kr_0^2(\beta = 1.7)$ $10^3 \times 24$	$Kr_0^2(\beta = 2.4)$ $8^3 \times 24$	$Kr_0^2(\beta = 2.4)$ $18^3 \times 24$	$Kr_0^2(\beta = 3.1)$ $16^3 \times 24$	Best estimate
3	1.25(8)	1.335(5)	1.32(1)	1.310(6)	1.324(4)(51)
8	2.60(1)	2.75(8)	2.60(3)	2.7(2)	2.602(9)(119)
6	2.9(2)	2.8(2)	3.00(3)	3.58(8)	3.06(3)(40)
15a	4.4(2)	4.1(2)	4.6(1)	5.7(3)	4.57(8)(82)
10	4.9(3)	4.7(2)	5.4(2)	7.5(2)	5.8(1)(16)
27	5.9(5)	7.0(4)	6.62(6)	8.2(4)	6.67(8)(116)
15s	7.1(5)	7.4(4)	7.6(2)	12.2(2)	9.5(1)(31)

TABLE IV. Best estimate of string tensions in energy units from different coupling constants. The ratio of string tensions is proportional to the ratio of Casimir scaling of the last column.

Rep.	K (GeV)	$\frac{K_r}{K_f}$	$\frac{C_r}{C_f}$
3	0.222(1)(8)(21)	-	-
8	0.437(2)(20)(42)	1.97(1)(12)	2.25
6	0.514(5)(67)(49)	2.32(3)(31)	2.5
15a	0.77(1)(15)(7)	3.47(5)(69)	4.0
10	0.97(2)(27)(9)	4.37(9)(123)	4.5
27	1.12(1)(20)(11)	5.05(5)(92)	6
15s	1.60(2)(52)(15)	7.2(1)(24)	7

TABLE V. Coulombic coefficients found by different lattice calculations and the best estimate. Rough agreement with Casimir ratios is observed.

Rep.	$A(\beta = 1.7)$ $10^3 \times 24$	$A(\beta = 2.4)$ $8^3 \times 24$	$A(\beta = 2.4)$ $18^3 \times 24$	$A(\beta = 3.1)$ $16^3 \times 24$	best estimate	$\frac{A_f}{A_r}$	$\frac{C_r}{C_f}$
3	-.40(8)	-.315(6)	-.330(9)	-.341(6)	-.329(4)(43)	-	-
8	-.60(5)	-.75(6)	-.93(3)	-.99(9)	-.84(2)(18)	2.55(7)(64)	2.25
6	-.54(9)	-.93(9)	-.69(6)	-.74(5)	-.72(3)(16)	2.2(1)(6)	2.5
15a	-.84(1)	-1.5(1)	-1.2(2)	-1.23(9)	-.85(1)(48)	2.58(4)(150)	4.0
10	-.50(2)	-1.6(2)	-.5(2)	-.7(1)	-.52(2)(63)	1.58(6)(193)	4.5
27	-1.9(5)	-1.6(2)	-1.71(6)	-2.5(2)	-1.76(6)(45)	5.4(2)(16)	6
15s	-1.6(4)	-2.3(2)	-2.1(2)	-1.95(6)	-1.98(6)(30)	6.0(2)(12)	7